# Phase relationships and structural, magnetic, and thermodynamic properties of the $Yb_5Si_4$-$Yb_5Ge_4$ pseudobinary system

Kyunghan Ahn,[1,2] A. O. Tsokol,[1] Yu. Mozharivskyj,[1] K. A. Gschneidner, Jr.,[1,2] and V. K. Pecharsky[1,2,*]
[1]*Ames Laboratory of the United States Department of Energy, Iowa State University, Ames, Iowa 50011-3020, USA*
[2]*Department of Materials Science and Engineering, Iowa State University, Ames, Iowa 50011-2300, USA*
(Received 15 March 2005; published 2 August 2005)

The crystallography, phase relationships, and physical properties of the $Yb_5Si_xGe_{4-x}$ alloys with $0 \leqslant x \leqslant 4$ have been examined by using single crystal and powder x-ray diffraction at room temperature, and dc magnetization and heat capacity measurements between 1.8 K and 400 K in magnetic fields ranging from 0 and 7 T. Unlike the majority of $R_5Si_xGe_{4-x}$ systems studied to date, where $R$ is the rare earth metal, all Yb-based germanide-silicides with the 5:4 stoichiometry crystallize in the same $Gd_5Si_4$-type structure. The magnetic properties of $Yb_5Si_xGe_{4-x}$ materials are nearly composition independent, reflecting the persistence of the same crystal structure over the whole range of $x$ from 0 to 4. Both the crystallographic and magnetic property data indicate that $Yb_5Si_xGe_{4-x}$ alloys are heterogeneous mixed valence systems, in which the majority (60%) of Yb atoms is divalent, while the minority (40%) is trivalent.

DOI: 10.1103/PhysRevB.72.054404 PACS number(s): 75.20.En, 75.20.Hr, 75.30.Cr, 61.66.Dk

## INTRODUCTION

When Smith *et al.*[1] discovered a few $R_5Si_4$ and $R_5Ge_4$ phases, where $R$ is rare earth metal, they reported that 5:4 germanides with $R$=Nd, Sm, Gd, Tb, Er, and Y, and the silicides with $R$=Tb, Er, and Y adopt the same orthorhombic crystal structure, while $Nd_5Si_4$ crystallizes in a tetragonal lattice. In a subsequent study by the same authors,[2] the crystal structure of the orthorhombic $Sm_5Ge_4$ was described as the $(ABCBA)_2$ stacking of three different sheets of atoms ($A$, $B$, and $C$) along the $b$ axis in space group symmetry *Pnma*. Within a few months, Smith, Tharp, and Johnson[3] reported that $R_5Ge_4$ compounds, where $R$=La, Ce—Sm, Gd—Tm, Lu, and Y, exhibit the same $Sm_5Ge_4$-type structure, while the crystallography of $R_5Si_4$ compounds is dependent upon the rare earth metal. Thus, $R_5Si_4$ with $R$=Sm, Gd, Tb, Dy, Er, and Y adopt the $Sm_5Ge_4$-type structure, but $R_5Si_4$ crystallize in the tetragonal $Zr_5Si_4$-type[4] lattice when $R$=La, Ce, Pr, and Nd. Nearly simultaneously with the structural work, Holtzberg *et al.*[5] reported that the $R_5Si_4$ phases, when $R$=heavy lanthanide, order ferromagnetically (FM) at relatively high Curie temperatures (i.e., $T_C$=336 K for $R$=Gd, 225 K for Tb, 140 K for Dy, 76 K for Ho, and 25 K for Er), while the $R_5Ge_4$ phases are antiferromagnetic (AFM) with much lower Néel temperatures, i.e., $T_N$=47 K for $R$=Gd, 30 K for Tb, 40 K for Dy, 21 K for Ho, and 7 K for Er. Authors of Ref. 5 also showed that substitutions of Si for Ge in $Gd_5Ge_4$ induce low-temperature ferromagnetism in the $Gd_5Ge_{4-x}Si_x$ solid solution.

In addition to complex crystallography and unusually large differences between the magnetic properties of the apparently isostructural $R_5Si_4$ and $R_5Ge_4$ compounds (e.g., high temperature FM $Gd_5Si_4$ vs low temperature AFM $Gd_5Ge_4$), combining magnetic Gd with just about the same amount of nonmagnetic Si increases the Curie temperature of the pure Gd metal ($T_C$=293 K) by nearly 40 K, i.e., $T_C$=336 K for $Gd_5Si_4$. Although this feature was noted by Holtzberg *et al.*[5] in 1967, and later reiterated by Elbicki *et al.*,[6] the $R_5T_4$ materials, where $T$=Si or Ge, did not attract much attention until 30 years later when Pecharsky and Gschneidner[7] reported the giant magnetocaloric effect (GMCE) in $Gd_5Si_2Ge_2$. The GMCE in this and many other members of the $Gd_5Si_xGe_{4-x}$ family of materials is due to first order magnetic phase transitions observed between ~40 K and ~300 K.[8] Importantly, the first order nature of these transformations is preserved in magnetic fields as high as 20 T.[9] Also in 1997, Pecharsky and Gschneidner[10] reported that there are three crystallographically different phase regions in the $Gd_5Si_xGe_{4-x}$ system at room temperature. For the $Gd_5Si_4$-based solid solution ($2 < x \leqslant 4$) and for the $Gd_5Ge_4$-based solid solution ($0 \leqslant x \leqslant 0.8$), they reported two different orthorhombic structures, but for the $Gd_5Si_2Ge_2$-type solid solution ($0.96 \leqslant x \leqslant 2$), there exists a monoclinically distorted lattice, which may be considered a 50:50 mixture of the structural features found in the corresponding 5:4 gadolinium silicide and in the 5:4 germanide. Authors of Ref. 10 believed that in the pseudobinary $Gd_5Si_4$—$Gd_5Ge_4$ system, the large differences in the magnetic properties, including the appearance of the GMCE, are intimately related to the crystallography of these three phases in the paramagnetic state.

Even though Smith *et al.*[1–3] reported that both $Gd_5Si_4$ and $Gd_5Ge_4$ adopt the orthorhombic $Sm_5Ge_4$-type structures, recent studies[11–13] describe them as equivalent layers of atoms assembled into slabs that are arranged in their own ways along the crystallographic $b$ direction because bonding between the slabs is distinctly different, e.g., see Fig. 1 in Ref. 12 and Ref. 14. The slabs themselves are formed by five nearly flat sheets of tightly bound atoms,[11,12] corresponding to the *ABCBA* sequence identified by Smith *et al.*[2] Hence, both the chemical and physical interactions between the slabs in the $Gd_5Si_xGe_{4-x}$ system vary with the chemical composition. For the $Gd_5Si_4$-type solid solution, all slabs are interconnected *via* $T_2$ dimers—the pairs of $T$ atoms from neighboring slabs at bonding distances of about 2.5 Å—and therefore, interactions between them are strong. For the $Gd_5Si_2Ge_2$-type solid solution, half of the interslab $T_2$ dimers

 

are broken (the bonding distances increase from ~2.5 to ~3.5 Å), thus, weakening the interslab exchange. Finally, for the $Gd_5Ge_4$-type solid solution, all interslab *T*-*T* bonds are broken, and these materials exhibit the weakest interslab exchange interactions, therefore, exhibiting the lowest magnetic ordering temperatures.

The family of $Gd_5Si_xGe_{4-x}$ alloys demonstrates a variety of unique physical phenomena related to magneto-structural transitions associated with reversible breaking and reforming of the interslab $T_2$ dimers that can be controlled by numerous external parameters such as chemical composition, magnetic field, temperature, and pressure.[12] When all interslab *T*-*T* bonds are present in the paramagnetic state, the alloys order ferromagnetically upon cooling without a structural change (second order phase transformation), see Fig. 2 in Ref. 12. However, when half or all of the interslab $T_2$ dimers are broken at room temperature, the alloys order ferromagnetically together with structural changes that restore all possible interslab $T_2$ dimers (first order phase transformation). The existence of the GMCE,[7] large magnetoresistance[15] and colossal magnetostriction[16] in $Gd_5Si_2Ge_2$ and related alloys, is therefore, intimately related to the combined magnetic-crystallographic transformations, e.g., see Fig. 3 in Ref. 12.

As far as the *R* component is of concern, $R_5Si_xGe_{4-x}$ systems with heavy lanthanides other than Gd have been investigated to some extent. Recently, phase diagrams of the pseudobinary systems with *R*=Tb,[17–19] Er,[20,21] and Y (Ref. 22) have been constructed. Selected $R_5Si_xGe_{4-x}$ compounds for *R*=La,[23,24] Pr,[25–27] Nd,[28–30] Tb,[31] Dy,[32] and Lu (Ref. 33) have been reported as well. Nonetheless, there are several $R_5Si_xGe_{4-x}$ systems, which have not been examined to date. For example, the $R_5T_4$ compounds for *R*=Eu have never been reported, and those for *R*=Ce,[34] Sm,[2] Tm,[3] and Yb (Refs. 35–37) have been examined only as binary intermetallics. Černý and Alami-Yadri[35] reported that $Yb_5Si_4$ adopts the orthorhombic $Gd_5Si_4$-type crystal structure, and noted a difference in the coordination of some of the *T* atoms compared to $Sm_5Ge_4$-type structure because all Si atoms in $Yb_5Si_4$ form covalently bonded pairs, while only one-half of the Ge atoms in $Sm_5Ge_4$ form covalent Ge-Ge bonds. Palenzona *et al.*,[36] and Pani and Palenzona,[37]on the other hand, state that both $Yb_5Si_4$ and $Yb_5Ge_4$ crystallize with the $Sm_5Ge_4$-type structure, thus fueling controversy about the room temperature crystallography of $Yb_5T_4$ compounds.

To date, only crystallographic data for the $Yb_5T_4$ binary compounds (*T*=Si or Ge) have been reported, but neither the physical properties nor the phase relationships in the $Yb_5Si_xGe_{4-x}$ system have been explored. In this work, we report on the phase relationships, structural, magnetic, and thermodynamic properties of several alloys belonging to the pseudobinary $Yb_5Si_xGe_{4-x}$ system. As we will show below, all binary and pseudobinary $Yb_5T_4$ compounds manifest characteristics of mixed valence systems. None of the studied alloys exhibit a structural transition concomitant with the magnetic ordering-disordering process, which is consistent with their crystallography where all of the slabs are already connected *via* the $T_2$) dimers in the paramagnetic state. All compounds with Yb order antiferromagnetically at low temperatures that are nearly independent of the Si:Ge ratio. This makes the $Yb_5Si_xGe_{4-x}$ system quite distinct compared to other $R_5Si_xGe_{4-x}$ systems studied to date.

## EXPERIMENT

A total of five alloys in the $Yb_5Si_xGe_{4-x}$ system with *x* varying from 0 to 4 were synthesized by induction melting at ~1800 °C with the holding time of 10 min. Prior to induction melting, stoichiometric mixtures of pure components (Yb, Si, and Ge) were loaded into Ta crucibles, and then the crucibles were sealed under pure helium atmosphere by arc welding in order to avoid losses of ytterbium due to the high vapor pressure of the metal. The Yb metal was prepared by the Materials Preparation Center of the Ames Laboratory and was 99.9 at. % (99.97 wt. %) pure with major impurities (in ppm atomic) as follows: Cl-380, C-245, Si-140, S-76, Al-62, O-49, Fe-43, Ca-35, and Lu-11. The silicon and germanium, which were purchased from a commercial vendor, were better than 99.999 wt. % pure. The alloy compositions were accepted in the as-weighed conditions because there were no weight losses during induction melting. The compositions $Yb_5Ge_4$, $Yb_5Si_2Ge_2$, and $Yb_5Si_3Ge$ were investigated in the as-cast conditions, without heat treatment. Two of the alloys, i.e., $Yb_5Si_4$ and $Yb_5SiGe_3$ were examined before and after they were heat treated at 1400 °C for 1 h.

The x-ray powder diffraction technique was utilized to characterize both the crystal structures and phase compositions of the $Yb_5Si_xGe_{4-x}$ alloys. The x-ray powder diffraction studies were performed on an automated Scintag powder diffractometer using Cu-$K\alpha$ radiation. The crystal structures were refined by the Rietveld technique.[38] Upon completion of the refinements, the profile residuals ($R_p$) were from 4.3% to 5.3%, and the derived Bragg residuals ($R_B$) were from 2.3% to 2.9%, indicating excellent fits of the adopted structural models to the observed experimental data.[39] For one of the alloys ($Yb_5SiGe_3$), the crystal structure was determined using single crystal x-ray diffraction data collected at room temperature using a Bruker SMART Apex CCD diffractometer with Mo $K\alpha$ radiation.

Magnetic measurements were performed using a SQUID magnetometer (model MPMS XL). The magnetization of zero-magnetic-field cooled samples was measured as a function of temperature from 1.8 to 400 K in various dc magnetic fields between 0.05 T and 5 T. Isothermal magnetization data were collected at 1.8, 2.5, and 10 K in dc magnetic fields varying from 0 to 7 T with 0.2 T steps after samples were zero field cooled to the target temperatures. The heat capacity of $Yb_5Ge_4$ was measured using an adiabatic heat-pulse calorimeter[40] between ~3.5 and 350 K in dc magnetic fields ranging from 0 to 7 T.

## RESULTS AND DISCUSSION

Systematic research, carried out since 1997, indicates that the crystallography of $R_5Si_xGe_{4-x}$ materials in the paramagnetic state is of extreme importance in order to understand and reconcile their physical, and especially, magnetic properties. Therefore, we will begin with the analysis of our room temperature diffraction data, followed by the description and relevant discussions of the basic magnetic and thermal properties of the $Yb_5Si_xGe_{4-x}$ materials.

TABLE I. Room temperature crystallographic data of $Yb_5Si_xGe_{4-x}$ alloys determined from the results of x-ray powder diffraction studies, unless indicated otherwise.

| Composition | Structure type | Unit cell dimensions, Å | | | Distance, $\delta_{T3\text{-}T3}$, Å | References |
|---|---|---|---|---|---|---|
| | | *a* | *b* | *c* | | |
| $Yb_5Si_4$ | $Gd_5Si_4$ | 7.26327(4) | 14.78061(8) | 7.70343(4) | 2.45(2) | 35 |
| $Yb_5Si_4$ | $Sm_5Ge_4$ | 7.262(2) | 14.784(4) | 7.700(2) | | 36 |
| $Yb_5Si_4$ | $Gd_5Si_4$ | 7.2695(3) | 14.7988(6) | 7.7103(3) | 2.49(2) | This work |
| $Yb_5Si_3Ge$ | $Gd_5Si_4$ | 7.2813(3) | 14.8183(5) | 7.7303(3) | 2.57(1) | This work |
| $Yb_5Si_2Ge_2$ | $Gd_5Si_4$ | 7.3035(4) | 14.8711(9) | 7.7661(5) | 2.64(1) | This work |
| $Yb_5SiGe_3$[a] | $Gd_5Si_4$ | 7.326(3) | 14.915(5) | 7.796(3) | 2.619(2) | This work |
| $Yb_5SiGe_3$ | $Gd_5Si_4$ | 7.3241(2) | 14.9220(3) | 7.8021(2) | 2.59(1) | This work |
| $Yb_5Ge_4$[a] | $Sm_5Ge_4$ | 7.342(2) | 14.958(1) | 7.828(1) | 2.65(2) | 37 |
| $Yb_5Ge_4$ | $Gd_5Si_4$ | 7.3406(5) | 14.9423(9) | 7.8253(5) | 2.65(1) | This work |

[a]Single crystal x-ray diffraction data.

## PHASE RELATIONSHIPS AND ROOM TEMPERATURE CRYSTALLOGRAPHY

Phase contents and room temperature crystal structures of all prepared alloys were determined using the x-ray powder diffraction technique and for one alloy using single crystal x-ray diffraction. The Rietveld refinements of the x-ray powder diffraction data resulted in precise lattice parameters (Table I), and the coordinates of individual atoms and, in most cases, occupancies of the *T* sites by the Si and Ge atoms (Table II). The observed and calculated (derived from the Rietveld refinements) powder diffraction patterns are shown in Figs. 1 and 2. The refinement results illustrated in Fig. 1 confirm that $Yb_5Si_4$, $Yb_5Si_3Ge$, $Yb_5Si_2Ge_2$, and $Yb_5Ge_4$ alloys are single phase materials within the sensitivity of the x-ray powder diffraction technique, which considering the quality of the data, was about 2 vol % of an impurity phase.[39]

One alloy, i.e., $Yb_5SiGe_3$, was not obtained in a single phase form. The main phase in this sample (71 wt. %, as determined from the Rietveld refinement) has the $Gd_5Si_4$-type structure, see Fig. 2 for the powder diffraction pattern of the two-phase alloy, Table I for the unit cell dimensions of the main phase, and Table II for the coordinates of atoms determined from a single crystal diffraction experiment. Both the as-prepared and heat treated $Yb_5SiGe_3$ contained significant amounts of an impurity phase which, as follows from the analysis of the powder diffraction data (Fig. 2), is a solid solution based on $Yb_{11}Ge_{10}$. The pure $Yb_{11}Ge_{10}$ germanide has a tetragonal $Ho_{11}Ge_{10}$-type[41] crystal structure with $a=10.72$ Å and $c=16.53$ Å.[42] The refined unit cell dimensions of the $Yb_{11}Si_xGe_{10-x}$ impurity are $a=10.6798(2)$ Å and $c=16.4262(6)$ Å, which are consistent with a solid solution where some of the larger Ge atoms are substituted by the smaller Si atoms. According to the Rietveld refinement, the chemical composition of the impurity is $Yb_{11}Si_{1.20(3)}Ge_{8.80(3)}$. This stoichiometry was obtained by refining site occupancies assuming that all five inequivalent Ge sites in the $Ho_{11}Ge_{10}$-type lattice are occupied by the identical statistical mixtures of Ge and Si atoms.

Since $Yb_5SiGe_3$ was not a single phase material, a complete x-ray diffraction study of a single crystal extracted from this alloy was undertaken in order to confirm the crystal structure of the compound and achieve a high precision in determining both the chemical composition and site occupancies in the $Yb_5T_4$ phase with as-weighed Si to Ge atomic ratio of 1:3. As follows from Table II, the stoichiometry of the majority phase is $Yb_5Si_{0.91(3)}Ge_{3.09(3)}$, i.e., it matches the as-weighed chemical composition to within three standard deviations. Some of the intraslab *T* sites (the *T*2 sites) are enriched in Si, while those that are responsible for the covalentlike interslab $T_2$ dimers (the *T*3 sites) accommodate more Ge compared to the 25 at. % Si and 75 at. % Ge expected for completely random occupancies of all corresponding *T* sites. Similar preferences in site occupancies have been earlier observed in $Gd_5Si_xGe_{4-x}$ with $x=2$,[11] and $x=0.44$, 1.28, and 1.84.[14] One unit cell of the $Yb_5SiGe_3$ crystal structure with its nearest surroundings highlighting the slabs, their stacking along the *b* axis and connectivity via the $T3_2$ dimers is shown in Fig. 3.

As the rare earth component changes through the $R_5Si_xGe_{4-x}$ series, three structurally distinct phase regions have been reported to exist as a function of *x* for the majority of *R*, i.e., for *R*=Y,[22] Pr,[25] Nd,[29] Gd,[10] Tb,[17] Dy,[33] and Er.[20] Two or more different phase regions exist when *R*=La,[33] and in one reported case, i.e., when *R*=Lu,[33] it appears that only the $Sm_5Ge_4$-type crystal structure persists as the number of Si atoms per formula unit changes from 0 to 4 in the $Lu_5Si_xGe_{4-x}$ system. Considering the results of the structural analysis presented above (Fig. 1, Fig. 2, Table I, and Table II), all studied $Yb_5Si_xGe_{4-x}$ alloys adopt the same $Gd_5Si_4$-type crystal structure regardless of *x*, as can be judged from similar unit cell dimension ratios and the nearly identical sets of coordinate triplets of all independent atoms. This structural identity reflects a continuous solid solubility between $Yb_5Si_4$ and $Yb_5Ge_4$ despite the fact that we were unable to prepare one of the alloys in a single phase form. The continuous solid solubility scenario is supported by the nearly linear behavior of the lattice parameters as functions of *x*, which is illustrated in Fig. 4. The appearance of the

TABLE II. Coordinates of atoms and *T*-site occupancies in $Yb_5Si_xGe_{4-x}$ alloys determined from the results of x-ray powder diffraction studies, unless indicated otherwise.

| Compound | Atom/site | *x*/*a* | *y*/*b* | *z*/*c* | *g* (%)[a] |
|---|---|---|---|---|---|
| $Yb_5Si_4$ | Yb1 in 4(*c*) | 0.3473(3) | $\frac{1}{4}$ | 0.0167(3) | |
| | Yb2 in 8(*d*) | 0.0216(2) | 0.0937(1) | 0.1784(2) | |
| | Yb3 in 8(*d*) | 0.3177(2) | 0.8778(1) | 0.1805(2) | |
| | Si1 in 4(*c*) | 0.254(2) | $\frac{1}{4}$ | 0.386(2) | 100 |
| | Si2 in 4(*c*) | 0.989(2) | $\frac{1}{4}$ | 0.868(2) | 100 |
| | Si3 in 8(*d*) | 0.148(1) | 0.9604(4) | 0.474(1) | 100 |
| $Yb_5Si_3Ge$ | Yb1 in 4(*c*) | 0.3457(3) | $\frac{1}{4}$ | 0.0159(3) | |
| | Yb2 in 8(*d*) | 0.0193(2) | 0.0940(1) | 0.1809(2) | |
| | Yb3 in 8(*d*) | 0.3191(2) | 0.8778(1) | 0.1745(2) | |
| | T1 in 4(*c*) | 0.239(1) | $\frac{1}{4}$ | 0.380(1) | 75[b] |
| | T2 in 4(*c*) | 0.979(1) | $\frac{1}{4}$ | 0.886(1) | 75[b] |
| | T3 in 8(*d*) | 0.1528(9) | 0.9626(3) | 0.4479(9) | 75[b] |
| $Yb_5Si_2Ge_2$ | Yb1 in 4(*c*) | 0.3425(3) | $\frac{1}{4}$ | 0.0192(3) | |
| | Yb2 in 8(*d*) | 0.0185(2) | 0.0941(1) | 0.1801(2) | |
| | Yb3 in 8(*d*) | 0.3193(2) | 0.8781(1) | 0.1747(2) | |
| | T1 in 4(*c*) | 0.2418(8) | $\frac{1}{4}$ | 0.3848(8) | 50(1)[c] |
| | T2 in 4(*c*) | 0.980(1) | $\frac{1}{4}$ | 0.882(1) | 63(1)[c] |
| | T3 in 8(*d*) | 0.1559(7) | 0.9603(2) | 0.4605(7) | 45.8(7)[c] |
| $Yb_5SiGe_3$[d] | Yb1 in 4(*c*) | 0.34312(6) | $\frac{1}{4}$ | 0.01791(6) | |
| | Yb2 in 8(*d*) | 0.01562(5) | 0.09372(3) | 0.18200(3) | |
| | Yb3 in 8(*d*) | 0.32015(4) | 0.87822(2) | 0.17330(4) | |
| | T1 in 4(*c*) | 0.2337(2) | $\frac{1}{4}$ | 0.3856(2) | 21.6(8)[c] |
| | T2 in 4(*c*) | 0.9741(2) | $\frac{1}{4}$ | 0.8791(2) | 34.1(8)[c] |
| | T3 in 8(*d*) | 0.1551(1) | 0.96027(7) | 0.4653(1) | 17.4(6)[c] |
| $Yb_5Ge_4$ | Yb1 in 4(*c*) | 0.3398(4) | $\frac{1}{4}$ | 0.0179(3) | |
| | Yb2 in 8(*d*) | 0.0167(3) | 0.0940(1) | 0.1826(2) | |
| | Yb3 in 8(*d*) | 0.3210(2) | 0.8781(1) | 0.1714(2) | |
| | Ge1 in 4(*c*) | 0.2299(8) | $\frac{1}{4}$ | 0.3852(7) | 100 |
| | Ge2 in 4(*c*) | 0.9736(9) | $\frac{1}{4}$ | 0.8780(7) | 100 |
| | Ge3 in 8(*d*) | 0.1555(6) | 0.9599(2) | 0.4619(6) | 100 |

[a]Occupancy by the Si atoms with the remainder (100% overall) occupied by the Ge atoms except for $Yb_5Ge_4$, where the value is for the site occupancies by the Ge atoms.

[b]The actual occupancies were not refined—they were assigned based on the as-prepared stoichiometry assuming completely random distribution of the Si and Ge atoms.

[c]Occupancies of the *T* sites have been refined with the only imposed constraint that each site has 100% overall occupancy.

[d]Single crystal x-ray diffraction data.

impurity phase at the $Yb_5SiGe_3$ stoichiometry (as-weighed) is likely a result of an accidental loss of a small amount of Yb to evaporation when the components were sealed inside a Ta crucible.

In Fig. 5, we show the variation of the lattice parameters of the orthorhombic $R_5Si_4$ and $R_5Ge_4$ compounds with $R$ =Gd through Lu. For the silicides, all of which have the same $Gd_5Si_4$-type structure (an old report[3] indicating a possibility of a monoclinic distortion in the $Lu_5Si_4$ lattice was not confirmed by a recent study[33]), a sharp increase in the *b* and *c* lattice parameters observed for $Yb_5Si_4$ is inconsistent with the normal lanthanide contraction assuming the uniform $R^{3+}$ valence states. For the germanides, the behaviors of the *b* and *c* axes follow those of the silicides, but the *a* axis of $Yb_5Ge_4$ exhibits a minimum. This minimum is in line with the differences in the crystallography of the ytterbium compound compared to the germanides with other heavy lanthanides. Similar anomalies in the lattice constants (and in the unit cell volumes) of Yb-containing compounds usually indicate that some or all of the Yb atoms in a material are either in the $Yb^{2+}$ or in a nonintegral, mixed valence state between $Yb^{3+}$ and $Yb^{2+}$. While the radii of the trivalent *R*

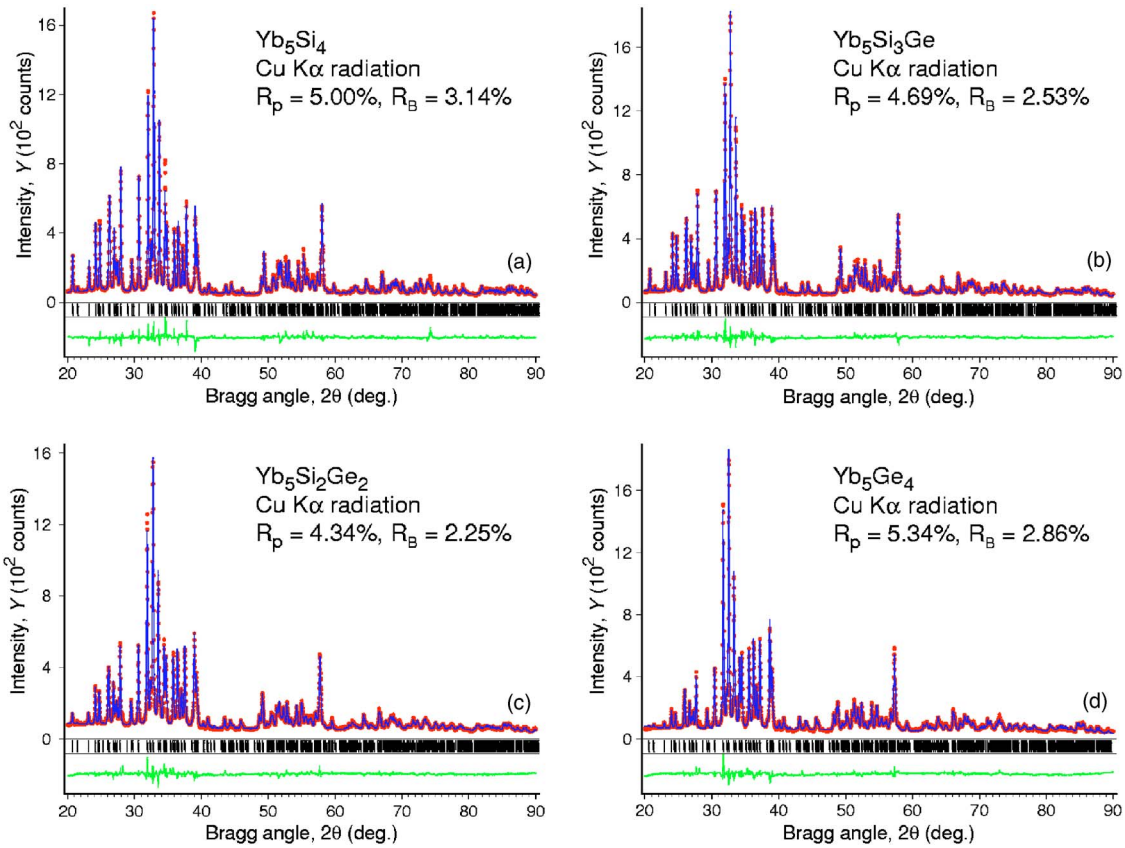


FIG. 1. (Color online) The observed (dots) and calculated (lines drawn through the data points) powder diffraction patterns of (a) $Yb_5Si_4$, (b) $Yb_5Si_3Ge$, (c) $Yb_5Si_2Ge_2$, and (d) $Yb_5Ge_4$ after the completion of Rietveld refinements. Calculated positions of the Bragg peaks are shown as vertical bars just below the plots of the observed and calculated intensities. The differences, $Y_{obs}-Y_{calc}$, are shown at the bottom of each plot.

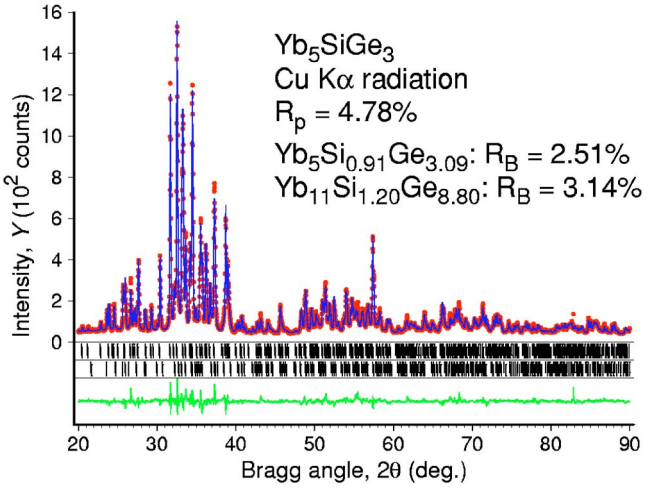


FIG. 2. (Color online) The observed (dots) and calculated (lines drawn through the data points) powder diffraction patterns of $Yb_5SiGe_3$ after the completion of Rietveld refinement. The upper set of vertical bars located just below the plots of the observed and calculated intensities indicates the calculated positions of the Bragg peaks of the majority $Yb_5Si_{0.91}Ge_{3.09}$ phase with the $Gd_5Si_4$-type structure, while the lower set of bars corresponds to the calculated positions of the Bragg peaks of the $Yb_{11}Si_{1.20}Ge_{8.80}$ impurity with the $Ho_{11}Ge_{10}$-type structure. The difference, $Y_{obs}-Y_{calc}$, is shown at the bottom of the plot.

ions decrease smoothly with the increasing atomic number due to the lanthanide contraction, the compounds in which Yb is in the pure 2+ state show large positive deviations from a smooth behavior. The lattice parameters of mixed valence compounds also deviate from the normal lanthanide contraction but the values of these deviations are intermediate between those observed for the two integral valence states. Thus, anomalies in the lattice constants of both $Yb_5Si_4$

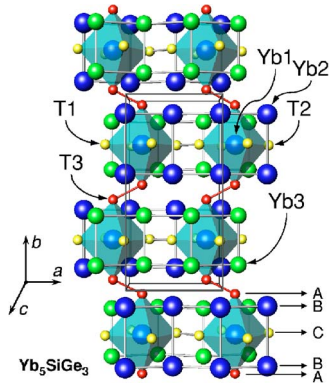


FIG. 3. (Color online) Perspective view of the crystal structure of $Yb_5SiGe_3$ along the $c$-axis highlighting both the slabs formed by stacking of five nearly flat atomic sheets *ABCBA* along the $b$ axis, (Ref. 2), and the existence of short $T3$-$T3$ dimers ($\delta_{T3\text{-}T3}$=2.62 Å).

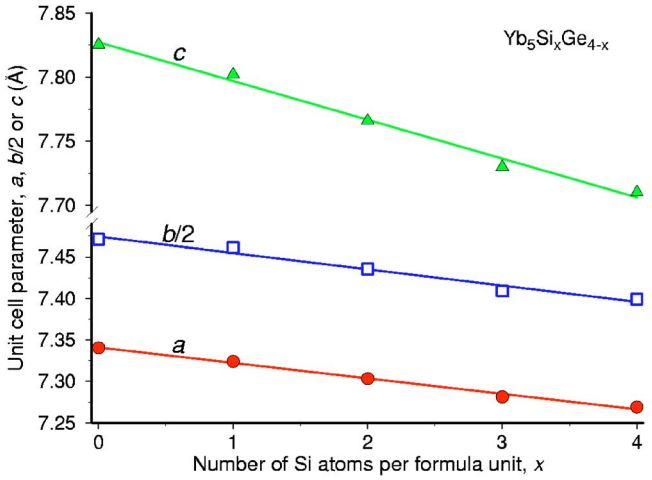


FIG. 4. (Color online) The behavior of the unit cell dimensions of $Yb_5Si_xGe_{4-x}$ as a function of $x$. Straight lines drawn through the data points are linear least squares fits.

and $Yb_5Ge_4$ indicate either the divalent or the mixed valence behavior of Yb in $Yb_5T_4$ compounds.

All things considered, the $Yb_5Si_xGe_{4-x}$ system is, therefore, quite different when compared to other $R_5Si_xGe_{4-x}$ systems studied to date. First, both the germanide and the silicide of ytterbium have the same $Gd_5Si_4$-type crystal structure, in which all (*ABCBA*) slabs are interconnected via the covalentlike $T_2$ dimers, whereas in the systems with other $R$ components, the germanide always has the $Sm_5Ge_4$-type structure, where all of the interslab dimers are broken. Second, the continuous solid solubility observed in the $Yb_5Si_xGe_{4-x}$ system is likely the result of the same crystallography of the 5:4 silicide and germanide of ytterbium. Finally, since crystallography in the paramagnetic state defines physical behaviors of the $R_5T_4$ compounds at low temperatures,[5–33] one might expect minimal changes of their magnetic and thermodynamic properties as a function of $x$ considering the structural stability within the $Yb_5Si_xGe_{4-x}$ family.

## MAGNETIC PROPERTIES

Considering that the amount of $Yb_{11}Si_{1.20(3)}Ge_{8.80(3)}$ impurity in the $Yb_5SiGe_3$ alloy was 29(1) wt. %, the physical properties of the latter were not measured. Samples extracted from all other alloys were subject to both the isofield and isothermal magnetization measurements. The low field ($B$=0.05 T) magnetization data collected on warming of the zero magnetic field-cooled samples, which are shown in Fig. 6, indicate that all alloys order antiferromagnetically at low temperatures. Néel temperatures, determined from the maxima of $M(T)$ functions, slowly increase from $T_N$=2.4 K for $Yb_5Si_4$ to $T_N$=3.2 K for $Yb_5Ge_4$. This behavior is contrary to that observed in all other $R_5Si_xGe_{4-x}$ systems ($R$=a magnetic lanthanide) studied to date, where the magnetic ordering temperatures decrease with decreasing Si content. Above ~50 K, the $B/M(T)$ functions of all $Yb_5Si_xGe_{4-x}$ compounds exhibit Curie-Weiss behaviors (see inset in Fig. 6).

Linear least squares fits of the data shown in the inset of Fig. 6 to $B/M=Np_{\text{eff}}^2/3k(T-\theta_p)$, where $B$ is the magnetic induction, $M$ is the molar magnetization, $N$ is Avogadro's number, $p_{\text{eff}}$ is the effective magnetic moment, $k$ is Boltzmann's constant, $T$ is the absolute temperature, and $\theta_p$ is the paramagnetic Curie-Weiss temperature, result in a nearly identical, composition-independent effective magnetic moment of the Yb atoms, see Table III and, for the most part, small and negative paramagnetic Curie-Weiss temperatures that are consistent with the AFM ground state of the materials. The only exception is small and positive $\theta_p$ for $Yb_5Si_3Ge$, yet the deviation of its value from zero is statistically insignificant considering experimental errors (±2 K). The average $p_{\text{eff}}=2.79(5)\mu_B$ is much smaller than the theoretical free ion effective magnetic moment of $Yb^{3+}$ ($4.54\mu_B$), which is usually taken as a convincing indicator that $Yb_5Si_xGe_{4-x}$ is a mixed-valence system. Normally, Yb atoms may exist in two valence states, $Yb^{2+}$ or $Yb^{3+}$. Since the electronic configuration of $Yb^{2+}$ is $4f$,[14] its total angular mo-

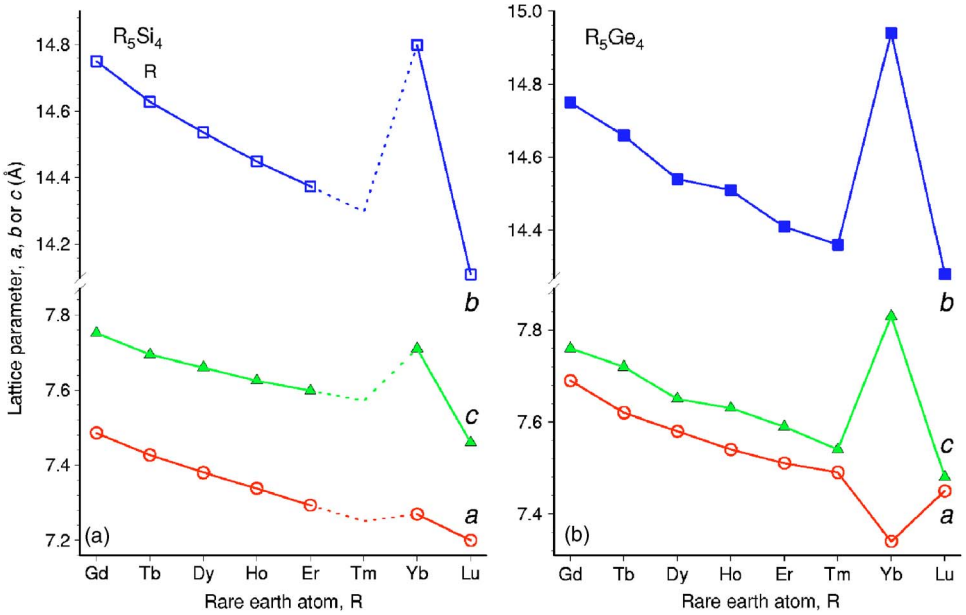


FIG. 5. (Color online) The unit cell dimensions of $R_5T_4$ silicides (a) and germanides (b) of heavy lanthanides as functions of the atomic number.

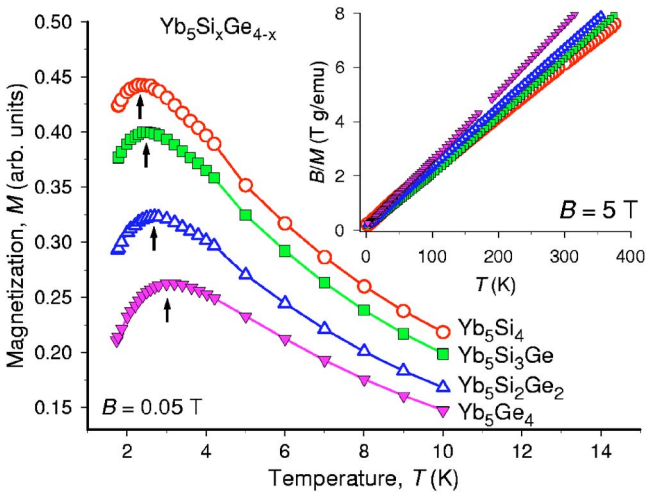


FIG. 6. (Color online) Low-magnetic field, low-temperature magnetization of zero magnetic field cooled samples of $Yb_5Si_xGe_{4-x}$ alloys measured on heating in a 0.05 T magnetic field. The arrows point to the maxima in the $M(T)$ behavior, which have been taken as Néel temperatures. The inset illustrates Curie-Weiss behavior of the inverse magnetization measured in a 5 T magnetic field.

mentum is $J=0$ resulting in $p_{\text{eff}}=0$, while $Yb^{3+}$ is in the $4f^{13}$ state with $J=7/2$. Assuming that there are two distinct valence states of Yb in the lattice, one can use the following expression in order to estimate the fraction of each ion: $p_{\text{eff}}=[zp^2_{\text{eff }1}+(1-z)p^2_{\text{eff }2}]^{1/2}$. Here, $p_{\text{eff}}$ is the observed effective magnetic moment per Yb ion, $p_{\text{eff }1}$ is the theoretical effective magnetic moment of the free $Yb^{2+}$ ion ($p_{\text{eff }1}=0$), $p_{\text{eff }2}$ is the theoretical effective magnetic moment of the free $Yb^{3+}$ ion ($p_{\text{eff }2}=4.54\mu_B$), and $z$ is the fraction of $Yb^{2+}$ ions. Solving with respect to $z$, the fractions of $Yb^{2+}$ ions in the unit cell vary from 0.64 for $Yb_5Ge_4$ to 0.61 for $Yb_5Si_4$ with the average $z=0.62(2)$, and those of $Yb^{3+}$ ions vary from 0.36 to 0.39 with the average of 0.38(2). Considering that there are a total of 20 Yb atoms per unit cell distributed among three inequivalent lattice sites (see Table II), it is easy to postulate that 12 out of 20 Yb atoms (60%) in each unit cell are in the $Yb^{2+}$ state, and 8 (40%) are in the $Yb^{3+}$ state. Although bulk magnetization measurements provide no clues with respect to which of the two 8($d$) Yb sites may accommodate the $Yb^{2+}$ ions, the crystallographic data of Table II may do so because of the difference in the atomic radii[43] ($r_{Yb^{2+}}=1.939$ Å, $r_{Yb^{3+}}=1.741$ Å). Analysis of the interatomic distances indicates that the Yb3 site is likely to accommodate the smaller $Yb^{3+}$ ions. These sites are shown as the medium size spheres in Fig. 3 (the medium size green spheres in the electronic version of this paper containing the colored illustrations). Both the anomalous behaviors of the unit cell dimensions (see above), and the magnetic properties of the $Yb_5Si_xGe_{4-x}$ compounds, therefore, indicate that the latter is a heterogeneous mixed valence family in which two crystallographically inequivalent Yb sites, i.e., Yb1 in 4($c$) and Yb2 in 8($d$), are occupied by the divalent Yb and one, Yb3 in 8[$d$], accommodates the trivalent Yb ions.

The isothermal magnetization behaviors of $Yb_5Si_xGe_{4-x}$ are shown in Fig. 7 as a function of the magnetic field, which was varied from 0 to 7 T at $T=1.8$ K and 10 K, i.e., they were measured just below and slightly above the Néel temperatures. The metamagnetic like behavior with $B_{cr}=1.3$ T (better seen as peaks in the insets displaying the derivatives of the magnetization with respect to the magnetic field), which is independent of alloy composition, is clearly visible at 1.8 K, thus indicating that the magnetic field induces spin-flip transformations in all of the alloys. Detectable, yet remanence-free hysteresis is observed both below and above $T_N$ when $x=4$ and $x=3$, but as the concentration of Ge increases, the $M(B)$ curves of alloys with $x=2$ and $x=0$ become nonhysteretic. Most likely, the gradual change of the hysteretic behavior reflects changes in domain wall pinning, and therefore, is related to a systematic variation of the microstructural features with $x$. For all $Yb_5Si_xGe_{4-x}$ alloys, the magnetization remains below $1.0\mu_B$/Yb atom in the magnetic field of 7 T. In fact, as shown in Table III, it remains below $2.4\mu_B/Yb^{3+}$ ion assuming that only eight out of every 20 Yb atoms are in the $Yb^{3+}$ state, and therefore, carry a moment. Considering that the expected saturated magnetic moment of $Yb^{3+}$ is $gJ=4.0\mu_B$, where $g$ is the gyromagnetic ratio and $J$ is the total angular momentum quantum number, the much lower values observed in the magnetically ordered state indicate that either the magnetic moments of $Yb^{3+}$ remain undeveloped down to 1.8 K or the magnetic structures of these $Yb_5Si_xGe_{4-x}$ compounds maintain complex noncollinear arrangements of fully developed magnetic moments of $Yb^{3+}$ even after the magnetic field-induced metamagnetic transitions. Resolution of this uncertainty will have to wait for a neutron scattering investigation of the microscopic details of the magnetic structure of a representative $Yb_5T_4$ compound.

## HEAT CAPACITY

The behavior of the heat capacity ($C_P$) of $Yb_5Ge_4$ measured on heating in various magnetic fields ranging from

TABLE III. Magnetic properties of $Yb_5Si_xGe_{4-x}$ alloys.

| Stoichiometry | $T_N$ (K) | $\theta_p$ (K) | $p_{\text{eff}}$ ($\mu_B$) | $Yb^{2+}$ ions per unit cell | $M$ at $T=1.8$ K, $B=7$ T, $\mu_B/Yb^{3+}$ |
|---|---|---|---|---|---|
| $Yb_5Si_4$ | 2.4 | −16 | 2.84 | 12.2 | 2.10 |
| $Yb_5Si_3Ge$ | 2.5 | 2 | 2.78 | 12.5 | 2.37 |
| $Yb_5Si_2Ge_2$ | 2.7 | −8 | 2.80 | 12.4 | 2.21 |
| $Yb_5Ge_4$ | 3.2 | −4 | 2.73 | 12.8 | 2.01 |

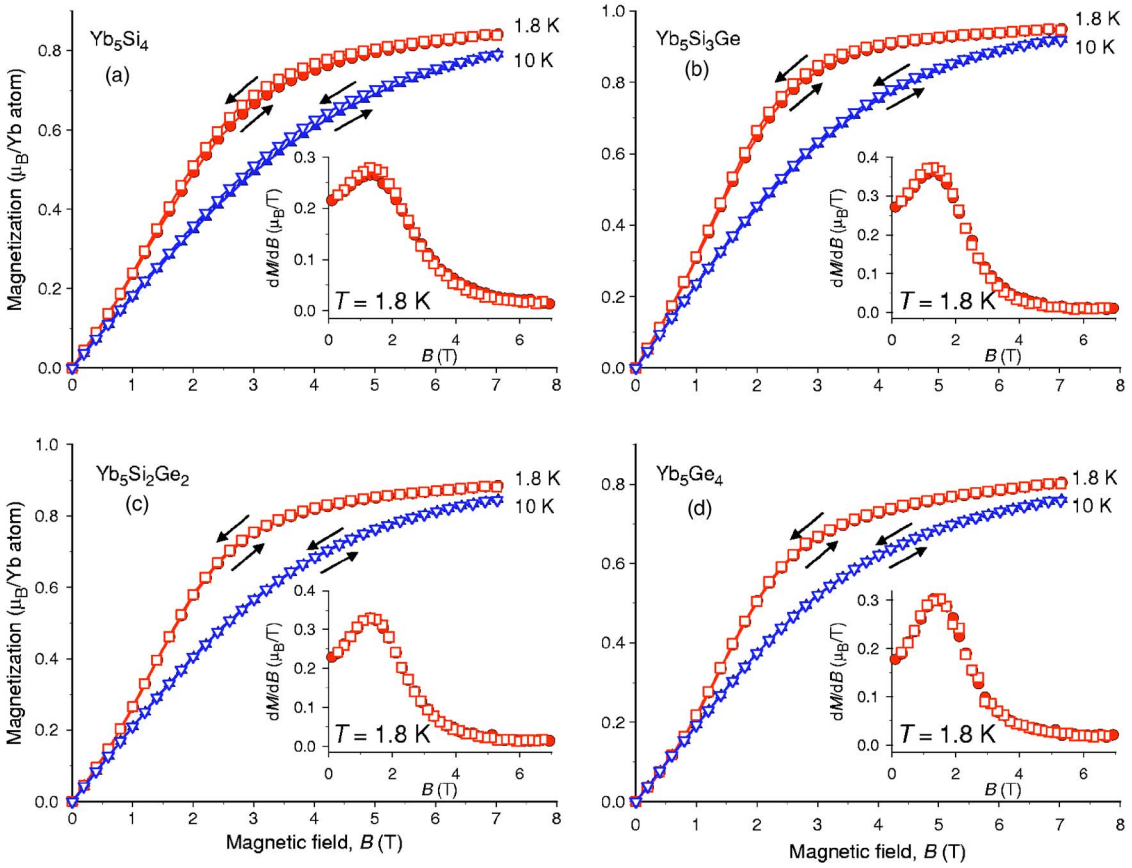


FIG. 7. (Color online) Magnetization of zero magnetic field cooled samples of $Yb_5Si_xGe_{4-x}$ alloys measured isothermally at 1.8 K and 10 K. The insets show the derivatives of the magnetization with respect to the magnetic field computed for the $T=1.8$ K data in order to illustrate the locations of the inflection points on each $M(B)$ curve.

0 to 7 T (Fig. 8) is consistent with the magnetization measurements. The upturn below ~9 K, observed in 0, 1 T, and 2 T magnetic fields, and the enhancement of $C_P$ over the range of temperatures exceeding 20 K in 5 T and 7 T fields, points to contributions other than normal lattice and electronic heat capacities. For comparison, we show the heat capacity of the nonmagnetic $Lu_5Ge_4$ on the same plot, which unfortunately, may only be considered as a rough approximation of the sum of the lattice and electronic components of $Yb_5Ge_4$ because the crystal structure of the compound with Lu (Refs. 3 and 33) is different from that of its ytterbium counterpart and that the valence of Lu is 3+, while it is 2.4+ for Yb. Weak magnetic fields (1 T and 2 T) have little effect on the low temperature heat capacity, which is consistent with the AFM ground state of the germanide (see Figs. 6 and 7). However, when the magnetic field is increased to 5 T and 7 T, which are considerably higher than the $B_{cr}=1.3$ T observed at $T=1.8$ K, the entropy of the system is shifted to high temperatures as expected for a magnetic field-induced FM-like state of $Yb_5Ge_4$.

The low temperature limit of our calorimeter is ~3.5 K, and therefore, we were unable to determine the shape of the zero-magnetic field heat capacity anomaly associated with the magnetic ordering of $Yb_5Ge_4$. Nonetheless, considerable enhancement of the heat capacity measured in a zero magnetic field at temperatures much higher than $T_N=3.2$ K is

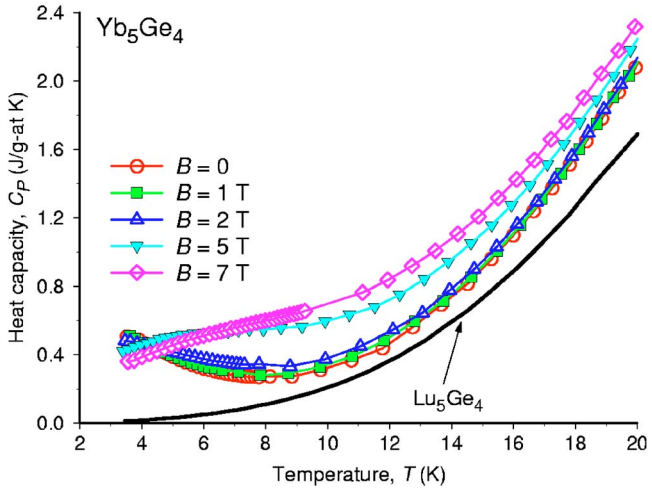


FIG. 8. (Color online) Low temperature heat capacity of $Yb_5Ge_4$ measured in 0, 1 T, 2 T, 5 T, and 7 T magnetic fields during heating of the zero magnetic field cooled sample. The lines drawn through the data points are guides for the eye. The thick solid line represents the heat capacity of the nonmagnetic $Lu_5Ge_4$, which is only a rough approximation of the lattice and electronic contributions in $Yb_5Ge_4$ because the crystal structures of these two germanides are different, as are the valences of Lu and Yb.

indicative of a second-order phase transformation, which is in line with a conventional order→disorder transition. Combined with the absence of a reliable lattice plus electronic specific heat baseline, this makes an estimate of the total magnetic entropy [theoretically, $\Delta S = R \ln(2J+1)$, which may have served as an additional proof that only eight out every 20 Yb atoms in the unit cell of $Yb_5Ge_4$ carry a magnetic moment], nearly impossible. Considering that the magnetic contribution to the total heat capacity in a zero magnetic field has been measured incompletely due to the low-temperature limit of the apparatus, the data shown in Fig. 8 are also unsuitable for an unbiased computation of the magnetocaloric effect.[44] Yet, taking into account the thermodynamic analysis performed by Pecharsky *et al.*,[45] it is easy to predict that the magnetocaloric effect of $Yb_5Ge_4$ will be negligible for magnetic field changes of 1 T and 2 T, and that the MCE will be strongly enhanced for $\Delta B = 5$ T and $\Delta B = 7$ T (in all cases, the magnetic field varies between 0 and the mentioned value). Furthermore, the high-field MCE of this compound should exhibit a conventional caretlike behavior with the maximum $|S_M|$ observed around 4.1 K and 4.5 K for magnetic field changes from 0 to 5 T and 0 to 7 T, respectively.

### $Yb_5Si_xGe_{4-x}$ VERSUS OTHER $R_5Si_xGe_{4-x}$ SYSTEMS

Among the eight heavy lanthanides (i.e., when $R$=Gd, Tb, Dy, Ho, Er, Tm, Yb, and Lu) all of the silicides at the $R_5Si_4$ stoichiometry (except Tm, for which no experimental data are available) crystallize in the $Gd_5Si_4$-type structure at room temperature. On the other hand, all germanides at the $R_5Ge_4$ stoichiometry adopt the $Sm_5Ge_4$-type structure at room temperature except Yb, which as follows from our investigation, belongs to the $Gd_5Si_4$ type. The major crystallographic difference between these two types of crystal structure is the presence of the covalentlike interslab $T$-$T$ dimers connecting the slabs in the $Gd_5Si_4$-type lattice as highlighted in Fig. 3, and their absence in the $Sm_5Ge_4$-type structure. Therefore, the lengths ($\delta$) of the interslab $T3$-$T3$ bonds are useful gauges to recognize either of these two structure types, in addition to the analysis of the $c/a$ ratios, which are larger for the $Gd_5Si_4$ type with the average $c/a = 1.036(5)$ compared to the $c/a = 1.010(3)$ for the $Sm_5Ge_4$-type lattice. Following Choe *et al.*,[14] the $\delta_{T3\text{-}T3}$ of ~2.6 Å between all of the slabs may be taken as an indicator of the $Gd_5Si_4$ type, the alternating ~2.6 Å and ~3.5 Å interslab $T3$-$T3$ distances manifest the monoclinic $Gd_5Si_2Ge_2$ type, and all interslab $\delta_{T3\text{-}T3}$ of ~3.5 Å signal the $Sm_5Ge_4$-type arrangement of the slabs. The room temperature crystallographic data for the $Yb_5Si_4$-$Yb_5Ge_4$ pseudobinary system tabulated in Tables I and II, confirm that all alloys with the $Yb_5Si_xGe_{4-x}$ stoichiometry crystallize in the $Gd_5Si_4$-type structure at room temperature, i.e., all of the slabs are interconnected *via* short, covalentlike Si(Ge)-Si(Ge) bonds. A systematic elongation of the interslab $\delta_{T3\text{-}T3}$ bonds from ~2.5 Å to ~2.6 Å, which occurs as $x$ changes from 4 to 0, is reflective of the differences in the effective radii of Si and Ge.

When divalent Yb is substituted for trivalent Gd in $R_5T_4$, the valence electron concentration in $Yb_5Si_xGe_{4-x}$ is lowered compared to $Gd_5Si_xGe_{4-x}$. This substitution, therefore, has a similar effect on the crystallography of $R_5T_4$ materials as when the tetravalent Ge is replaced by the trivalent Ga in $Gd_5Ge_{4-x}Ga_x$.[46] As the concentration of Ga increases in the latter, the $Sm_5Ge_4$-type structure adopted by the pure germanide ($x=0$, valence electron concentration is 31 $e^-$/formula unit) is first replaced by the $Pu_5Rh_4$ type when $x=1$, which corresponds to 30 valence electrons/formula unit. The $Pu_5Rh_4$-type lattice is intermediate between the $Sm_5Ge_4$ and $Gd_5Si_4$ types of crystal structure, as was judged by the evolution of the interslab $\delta_{T3\text{-}T3}$ distances.[46] Upon a further increase of the Ga concentration, the $Gd_5Si_4$-type lattice becomes stable when $x=2$, corresponding to the formal valence electron count of 29 valence electrons/formula unit. Counting valence electrons in $Yb_5Si_xGe_{4-x}$ materials results in the total of 28 valence electrons per formula unit, thus explaining the stability of the $Gd_5Si_4$-type structure regardless of $x$ when $R$=Yb. Even though the valence electron concentration argument may be considered artificial, the structural behavior exhibited by the $Yb_5Si_xGe_{4-x}$ system confirms that low valence electron count results in the stabilization of the $T$-$T$ dimers. In this regard, replacing some of the Si atoms by P, Sb, or As may result in weakening of the interslab interactions, thus providing additional chemical tools in tuning both the crystallography and physical properties of this particular intermetallic system, as well as of other $R_5T_4$ materials.

Considering the magnetic properties of $R_5T_4$ compounds, the silicides with $R$=Gd, Tb, Dy, Ho, and Er, order ferromagnetically but the germanides with the same rare earth ions, are antiferromagnets at low temperatures (see Refs. 5–37). Carried over into the ternary silicide-germanide $R_5Si_xGe_{4-x}$ systems with $R$=Gd through Er, this difference in the magnetic behaviors of the binary parent compounds results in discontinuous changes of the magnetic ground states at different $R$-specific concentrations, $x$. However, as follows from this study, the ground states of the ytterbium silicide and the germanide are nearly identical—both order antiferromagnetically at about the same low temperature of ~3 K. The low magnetic ordering temperatures in the $Yb_5Si_xGe_{4-x}$ system are likely related to the fact that the majority of Yb atoms are the nonmagnetic $Yb^{2+}$ ions. Another peculiarity of the $Yb_5Si_xGe_{4-x}$ system is that the magnetic coupling here always remains AFM regardless of the presence of the covalentlike interslab $T3$-$T3$ bonds. Although indirectly, this result supports the notion[12] about the [-$T$-$R$-$T$-$T$-$R$-$T$-] superexchange playing a role in enhancing the FM coupling between the slabs. It is easy to see (Fig. 3, and the discussion of valence states of different Yb sites, above) that even though the covalent like chains [-T3-Yb1-T3-T3-Yb1-T3-] do exist in all of the $Yb_5Si_xGe_{4-x}$ alloys, their effect on the magnetic interactions is negligible because the Yb1 sites are occupied by the nonmagnetic $Yb^{2+}$ ions.

## CONCLUSIONS

In summary, $Yb_5Si_xGe_{4-x}$ alloys preserve the same crystal structure as $x$ varies from 4 to 0, which leads to a continuous solid solubility between $Yb_5Si_4$ and $Yb_5Ge_4$. As a result,

replacements of Ge by Si and vice versa have little effect on the magnetic properties of materials, which is a unique feature compared to all other $R_5T_4$ systems formed by lanthanides with incompletely filled $4f$ shells. Three different lattice sites accommodating lanthanides in the $Gd_5Si_4$-type crystal structure exhibit selectivity with respect to the valence states of Yb ions. The nonmagnetic $Yb^{2+}$ ions are located in the $4(c)$ and one of the $8(d)$ sites, while the $Yb^{3+}$ ions are located exclusively in the $8(d)$ sites. $Yb_5Si_xGe_{4-x}$, therefore, may be considered to be a heterogeneous mixed valence system. All $Yb_5Si_xGe_{4-x}$ alloys exhibit weak AFM correlations at temperatures between 2.4 K and 3.2 K

## ACKNOWLEDGMENT

This work was supported by the Office of Basic Energy Sciences, Materials Sciences Division of the U.S. Department of Energy under Contract No. W-7405-ENG-82 with Iowa State University.

*Electronic address: vitkp@ameslab.gov

[1] G. S. Smith, A. G. Tharp, and Q. Johnson, Nature (London) **210**, 1148 (1966).
[2] G. S. Smith, Q. Johnson, and A. G. Tharp, Acta Crystallogr. **22**, 269 (1967).
[3] G. S. Smith, A. G. Tharp, and Q. Johnson, Acta Crystallogr. **22**, 940 (1967).
[4] H.-U. Pfeifer and K. Schubert, Z. Metallkd. **57**, 884 (1966).
[5] F. Holtzberg, R. J. Gambino, and T. R. McGuire, J. Phys. Chem. Solids **28**, 2283 (1967).
[6] J. M. Elbicki, L. Y. Zhang, R. T. Obermeyer, and W. E. Wallace, J. Appl. Phys. **69**, 5571 (1991).
[7] V. K. Pecharsky and K. A. Gschneidner, Jr., Phys. Rev. Lett. **78**, 4494 (1997).
[8] V. K. Pecharsky and K. A. Gschneidner, Jr., Appl. Phys. Lett. **70**, 3299 (1997).
[9] F. Casanova, A. Labarta, X. Batlle, J. Marcos, L. Mañosa, A. Planes, and S. de Brion, Phys. Rev. B **69**, 104416 (2004).
[10] V. K. Pecharsky and K. A. Gschneidner, Jr., J. Alloys Compd. **260**, 98 (1997).
[11] W. Choe, V. K. Pecharsky, A. O. Pecharsky, K. A. Gschneidner, Jr., V. G. Young, Jr., and G. J. Miller, Phys. Rev. Lett. **84**, 4617 (2000).
[12] V. K. Pecharsky and K. A. Gschneidner, Jr., Adv. Mater. (Weinheim, Ger.) **13**, 683 (2001).
[13] V. K. Pecharsky, A. O. Pecharsky, and K. A. Gschneidner, Jr., J. Alloys Compd. **344**, 362 (2002).
[14] W. Choe, A. O. Pecharsky, M. Worle, and G. J. Miller, Inorg. Chem. **42**, 8223 (2003).
[15] L. Morellon, J. Stankiewicz, B. García-Landa, P. A. Algarabel, and M. R. Ibarra, Appl. Phys. Lett. **73**, 3462 (1998).
[16] L. Morellon, P. A. Algarabel, M. R. Ibarra, J. Blasco, B. García-Landa, Z. Arnold, and F. Albertini, Phys. Rev. B **58**, R14721 (1998).
[17] C. Ritter, L. Morellon, P. A. Algarabel, C. Magen, and M. R. Ibarra, Phys. Rev. B **65**, 094405 (2002).
[18] L. Morellon, C. Ritter, C. Magen, P. A. Algarabel, and M. R. Ibarra, Phys. Rev. B **68**, 024417 (2003).
[19] L. Morellon, Z. Arnold, C. Magen, C. Ritter, O. Prokhnenko, Y. Skorokhod, P. A. Algarabel, M. R. Ibarra, and J. Kamarad, Phys. Rev. Lett. **93**, 137201 (2004).
[20] A. O. Pecharsky, K. A. Gschneidner, Jr., V. K. Pecharsky, D. L. Schlagel, and T. A. Lograsso, Phys. Rev. B **70**, 144419 (2004).
[21] J. M. Cadogan, D. H. Ryan, Z. Altounian, X. Liu, and I. P. Swainson, J. Appl. Phys. **95**, 7076 (2004).
[22] A. O. Pecharsky, V. K. Pecharsky, and K. A. Gschneidner, Jr., J. Alloys Compd. **379**, 127 (2004).
[23] H. F. Yang, G. H. Rao, W. G. Chu, G. Y. Liu, Z. W. Ouyang, and J. K. Liang, J. Alloys Compd. **334**, 131 (2002).
[24] H. F. Yang, G. H. Rao, G. Y. Liu, Z. W. Ouyang, W. F. Liu, X. M. Feng, W. G. Chu, and J. K. Liang, J. Alloys Compd. **361**, 113 (2003).
[25] H. F. Yang, G. H. Rao, W. G. Chu, G. Y. Liu, Z. W. Ouyang, and J. K. Liang, J. Alloys Compd. **339**, 189 (2002).
[26] H. F. Yang, G. H. Rao, G. Y. Liu, Z. W. Ouyang, W. F. Liu, X. M. Feng, W. G. Chu, and J. K. Liang, J. Magn. Magn. Mater. **263**, 146 (2003).
[27] G. H. Rao, Q. Huang, H. F. Yang, D. L. Ho, J. W. Lynn, and J. K. Liang, Phys. Rev. B **69**, 094430 (2004).
[28] J. M. Cadogan, D. H. Ryan, Z. Altounian, B. H. Wang, and I. P. Swainson, J. Phys.: Condens. Matter **14**, 7191 (2002).
[29] H. F. Yang, G. H. Rao, G. Y. Liu, Z. W. Ouyang, W. F. Liu, X. M. Feng, W. G. Chu, and J. K. Liang, J. Alloys Compd. **346**, 190 (2002).
[30] C. Magen, L. Morellon, P. A. Algarabel, M. R. Ibarra, C. Ritter, A. O. Pecharsky, K. A. Gschneidner, Jr., and V. K. Pecharsky, Phys. Rev. B **70**, 224429 (2004).
[31] L. Morellon, Z. Arnold, C. Magen, C. Ritter, O. Prokhnenko, Y. Skorokhod, P. A. Algarabel, M. R. Ibarra, and J. Kamarad, Phys. Rev. Lett. **93**, 137201 (2004).
[32] V. V. Ivtchenko, V. K. Pecharsky, and K. A. Gschneidner, Jr., Adv. Cryog. Eng. **46A**, 405 (2000).
[33] K. A. Gschneidner, Jr., V. K. Pecharsky, A. O. Pecharsky, V. V. Ivtchenko, and E. M. Levin, J. Alloys Compd. **303**, 214 (2000).
[34] M. V. Bulanova, P. N. Zheltov, K. A. Meleshevich, P. A. Saltykov, and G. Effenberg, J. Alloys Compd. **345**, 110 (2002).
[35] R. Černý and K. Alami-Yadri, Acta Crystallogr., Sect. E: Struct. Rep. Online **59**, i1 (2003).
[36] A. Palenzona, P. Manfrinetti, S. Brutti, and G. Balducci, J. Alloys Compd. **348**, 100 (2003).
[37] M. Pani and A. Palenzona, J. Alloys Compd. **360**, 151 (2003).
[38] B. A. Hunter, Rietica—A visual Rietveld program, International Union of Crystallography Commission on Powder Diffraction, Newsletter No. 20 (Summer, 1998) http://www. rietica. org.
[39] V. K. Pecharsky and P. Y. Zavalij, *Fundamentals of Powder Diffraction and Structural Characterization of Materials* (Kluwer Academic, New York, 2003).
[40] V. K. Pecharsky, J. O. Moorman, and K. A. Gschneidner, Jr., Rev. Sci. Instrum. **68**, 4196 (1997).
[41] A. G. Tharp, G. S. Smith, and Q. Johnson, Acta Crystallogr. **20**,

583 (1966).

[42] V. N. Eremenko, K. A. Meleshevich, and Y. I. Buyanov, Dopov. Akad. Nauk. Ukr. RSR, Ser. A: Fiz.-Mat. Tekh. Nauki **1983**, 83 (1983).

[43] E. T. Teatum, K. A. Gschneidner, Jr., and J. T. Waber, Compilation of calculated data useful in predicting metallurgical behavior of the elements in binary alloy systems, Los Alamos Scientific Laboratory Report No. LA-4003, 1968, National Technical Information Service, U. S. Department of Commerce, Springfield, VA 22161.

[44] V. K. Pecharsky and K. A. Gschneidner, Jr., J. Appl. Phys. **86**, 565 (1999).

[45] V. K. Pecharsky, K. A. Gschneidner, Jr., A. O. Pecharsky, and A. M. Tishin, Phys. Rev. B **64**, 144406 (2001).

[46] Yu. Mozharivskyj, W. Choe, A. O. Pecharsky, and G. J. Miller, J. Am. Chem. Soc. **125**, 15183 (2003).